Vertical profiling of atmospheric air pollutants in rural India: A case study on particulate matter (PM10/PM2.5/PM1), carbon dioxide, and formaldehyde

Vertical profiling of atmospheric air pollutants in rural India: A case study on particulate matter (PM_{10}/$PM_{2.5}$/PM_1), carbon dioxide, and formaldehyde

Sneha Gautam[1*], Cyril Sammuel[1], Aniket Bhardwaj[1], Zahra Shams Esfandabadi[2,3], M Santosh[4,5], Alok Sagar Gautam[6*], Abhishek Joshi[6], Aldin Justin[1], G. Jims John Wessley[1], E J James[1]

1Karunya Institute of Technology and Sciences, Coimbatore, 641114, Tamil Nadu, India

2Department of Environment, Land and Infrastructure Engineering (DIATI), Politecnico di Torino, Corso Duca degli Abruzzi 24, 10129 Torino, Italy

3Energy Center Lab, Politecnico di Torino, Via Paolo Borsellino 38/16, 10138 Torino, Italy

4School of Earth Sciences and Resources, China University of Geosciences Beijing, Beijing 100083, China

5Department of Earth Science, University of Adelaide, Adelaide SA 5005, Australia

6Hemvati Nandan Bahuguna Garhwal University, Srinagar,Garhwal, Uttarakhand, 246174, India

*Corresponding Author:

Dr. Sneha Gautam

Email ID: snehagautam@karunya.edu / gautamsneha@gmail.com / phyalok@gmail.com

Vertical profiling of atmospheric air pollutants in rural India: A case study on particulate matter ($PM_{10}/PM_{2.5}/PM_1$), carbon dioxide, and formaldehyde

Abstract

Particulate matter is one of the major air pollutants that challenge the environment and human health. In this study, we used an unmanned aerial vehicle associated with smart, low-cost sensors to record the vertical profiles of particulate matters (PM_{10}/ $PM_{2.5}$/ PM_1), carbon dioxide, and formaldehyde in a rural area of southern India. Our study covered the surface to 60 m above the ground level compiling data over twenty days of measurements in March 2021. A total of thirty flights were performed in the five selected locations. The data show a decrease in air pollutant concentration with increasing height from the surface. However, statistical data analysis through CHAID Decision Trees and 3-D visualization of the relationship between the pollutants and the height, RH, and temperature show that the concentration of pollutants is more strongly influenced by the location and meteorological parameters rather than the height from the surface. We infer that transport through both advection and convection influences the vertical distribution of air pollutants as inferred from meteorological analysis, including back trajectories using the Hybrid Single-Particle Lagrangian Integrated Trajectory (HYSPLIT4) model. The long-range transport of air mass could also contribute to the high concentration values of particulate matters, as found through the five-day air mass backward trajectory analysis. Although the observed data sets are confined to a height of 60 m AGL, the results from this study provide insights into the vertical

distribution of air pollutants, complementing ground-based measurement variations with different spacing and timing.

Keywords: Particulate matter vertical profile; CO_2; Formaldehyde; Unmanned aerial vehicle; Rural India.

1. Introduction

Our planet's environment is affected by various air pollutants in the atmosphere, particularly as a result of anthropogenic activities (e.g., Li et al., 2015; Silva et al., 2021; Gollakota et al., 2021). The particulate matter with different sizes affects climate change and visibility by reducing the light as well as altering the atmospheric radiative budget (Wang et al., 2015; Praveen et al., 2012). Air pollutants have also significantly severely impacted the life and environment (Lei et al. 2016; Bond et al. 2013). Among these, formaldehyde, an organic component, has been shown to cause serious health issues (Vardoulakis et al. 2020).

Ground-based measurements of particulate matter have been reported in several previous studies (Ravina et al., 2021; Liu et al., 2019; Retama et al., 2015; Gautam et al. 2016; Patra et al. 2016; Klompmaker et al., 2015). TA variation in chemical composition, size distribution, and mass concentration of air pollutants at different heights in the urban atmosphere has also been reported (Lu et al. 2016; Minguillón et al. 2015; Ferrero et al. 2010). The upward movement, dispersion, diffusion, accumulation, and deposition of the particle are also influenced by planetary boundary layers (Tang et al., 2016; Gautam et al. 2015). Thus, studies on the vertical profile of air pollutants are critical to assess the air pollutant concentration at different heights and their spatial characteristics, especially in the rural atmosphere. Various techniques such as Tethered balloons, remote sensing, meteorological towers, and human-made aircraft were employed to assess the vertical distribution of air pollutants in different geographic regions (Ran et al. 2016; Han et al. 2015; Ding et al. 2009; Strawbridge and Snyder 2004). Unmanned Aerial Vehicles (UAVs) provides one of the robust and alternative methods with high-cost efficiency, flexibility, and mobility to assess the vertical behavior of air pollutants (Schuyler and Guzman, 2017; Villa et al. 2016).

Previous studies which investigated air pollutant concentration / vertical distribution by using UAVs (Bates et al. 2013) reported notable variation in the distribution patterns of particle concentration. Some studies reported contrasting results of higher concentrations with increasing height causing enhanced light absorption (Bates et al. 2013) or decreasing trend of fine particles with increasing height (Zhu et al. 2019). Some researchers (Chilinski et al. 2016; Ran et al. 2016; Ferrero et al. 2011) have observed lower air pollutants concentration above the planetary boundary layer (PBL) compared to ground level under clean conditions. Some of the recent studies (Lu et al. 2019; Ran et al. 2016) correlated these features to local emissions or local fossil fuel combustion sources rather than the long-range transport sources. Peng et al. (2015) highlighted that the vertical profile (300 and 1000 m above the ground level) of air pollutants, especially $PM_{2.5}$, might be affected significantly by diurnal variation of temperature. However, one of the limitations in most of these studies is the limited number of days/flights and the restricted data on specific pollutants. Comprehensive investigations to understand the relationship between contaminants and atmospheric stability are rare.

Analysis of the vertical distribution of such pollutants is necessary to understand the emission sources, residence period, and dispersion of pollutants in the atmosphere. Most contaminants are emitted from the ground sources and are usually limited to the lower atmosphere, within the PBL

(Samad et al., 2020), and the heights vary throughout the daytime, subject to atmospheric conditions.

Pollutants from different sources get mixed, and their vertical distribution varies diurnally with height. This layer in the lower atmosphere is termed a mixing layer (Baumbach 1996). Studies have shown that the stability of PBL can reduce the mixing of pollutants due to the stable atmosphere governed by wind speed and solar radiation (Zoras et al., 2006). Higher air pollution episodes were reported previously during the temperature inversion in the lower atmosphere over different geographical conditions (Janhall et al., 2006; Baumbach and Vogt, 2003; Silva et al., 2007; Olofson et al., 2009; Guzmán-Torres et al., 2009; Panday and Prinn, 2009). Temperature inversion hinders the convective air movement, and also restricts the dispersion of pollutants and confines the pollutants within the limited air mass (Allaby 2007). This study was undertaken with a view to assess the vertical distribution of pollutants and meteorological parameters and to understand the temperature inversion and its impact on pollution over the study region.

Here we investigate the vertical profile distribution of major pollutants (i.e., formaldehyde (HCHO), carbon dioxide (CO_2), and fine particulate matter (PM)) with meteorological conditions to explore the vertical distribution pattern of air pollutants (i.e., PM_{10}, $PM_{2.5}$, PM_1, CO_2, & HCHO) in a rural area of southern India. In the present study, we measured the vertical profile of air pollutants (PM_{10}, $PM_{2.5}$, PM_1, CO_2, & HCHO) using UAVs (450 mm 3s quad multi-rotor setup) for 12 days in March 2021 at the Karunya Institute of Technology and Sciences, Karunya Nagar, Coimbatore, India. A total of 30 flights were employed at five different locations of the university area with a height of 15 m, 30 m, 45 m, and 60 m (regulated by the DGCA (Directorate General of Civil Aviation) above ground level between 08:00 am - 12:00 pm local time. The selected study area is located approximately 28 km away from the urban area (Coimbatore city), thus providing an opportunity to investigate the effects of meteorological parameters (i.e., temperature and relative humidity) and regional transport on the local air pollution. Building Decision-trees (DTs) in IBM® SPSS® software, the strength and effect of meteorological parameters and concentration of the pollutants with height were evaluated for each of the five sampling locations. Furthermore, the vertical distribution of air pollutants was visualized using the Fuzzy toolbox in MATLAB® to understand how the atmospheric stability and layers influence pollutants' behavior at a vertical scale. Our study reveals the influence of temperature and relative humidity. We also present and evaluate cases with transportation influence from the main road (~ 1 km),

2. Material and methods

2.1 Site Description and Experiment Design

Karunya Nagar is in a rural area located within the Tamil Nadu State of southern India (Fig. 1 1), around 30 km from the densely populated Coimbatore city. The study was piloted at the campus of the Karunya University of Technology and Sciences (10.93620N, 76.74410E). By following the regulation of DGCA, 30 successive flights were undertaken inside and outside the campus. The duration of each round trip of flight (0 – 15m – 30m – 45m – 60 m from the ground and back) was 10 minutes. Before each flight, ground-based measurement was conducted for 5 minutes.

2.2 UAVs platform and instruments

In this study, we conducted vertical monitoring by using a UAV (450mm 3s quad multi-rotor setup). The drone moved upward in the direction from the ground to 60 m above ground level at a constant speed of 1 m/s and then descended along the same path at the same rate. The total developed payload was mounted on the drone for conducting air pollutant and meteorological parameters (i.e., temperature and relative humidity) measurements. All sensors were mounted on the UAV to minimize the influence of the downwash effects (Zhou et al., 2018).

The sensor (Prana Air – CIA+) is used for pollution measurement. The "Prana Air – CIA+" was mounted on a quad configuration multi-rotor of 450 mm dimension, which runs on a 35 (12.6 V 3800 mah) lipo battery producing an appropriate flying time of 15 minutes. The multi-rotor combined with 10 inches propellers and 900 kV high torque BLDC (Brushless DC) motor can lift 1.5 kg of payload in Air. The brain of the multi-rotor (ic) flight controller used in the setup is DJI NAZA H LITE, which offers a steady flight to perform the flight plan. The GPS (Global Positioning System) integrated with the flight controller helps in a stable flight, and features like RTL, failsafe, altitude lock and GPS lock make the flight highly functional. Used an additional flight controller (JHEHCU FTBT) to obtain live altitude telemetry using the JHEHCU FTBT flight controller's barometric sensor. The flight controller also has an OSD (On Screen Display Chip) and an additional intractable camera (RUNCAH Micro Swift 2 600 TVL) and AKK VTX (video transmitter) of 5.8GHz band. The VTX transmits the on-flight footage and OSD data to a 5.8 GHz video receiver connected to an android device.

Cluster analysis of air mass trajectories is used to find the contribution function of potential sources of pollutants (Argyropoulos et al., 2013). This approach also provides information on the pathways and flow patterns of air mass followed before reaching the observation site (Borbély-Kiss et al., 1999). Trajectory statistics and transport models combined with satellite or ground-based observations provide spectral and temporal distribution of pollutants and improve the forecast of air quality (Mijling et al., 2012). Cluster analysis of five days' air mass back trajectories was performed using the Hybrid Single-Particle Lagrangian Integrated Trajectory (HYSPLIT4) model (Stein et al., 2015). The meteorological data for the trajectory calculation is obtained from

NOAA's Global Data Assimilation System (GDAS, 1˚ × 1˚). All trajectories were calculated at 500 m above ground level (AGL) ending at the observation site (10.94° N, and 76.74° E) for the observation period between 5 Mar 2021 to 17 Mar 2021. A multivariate statistical tool (Cluster analysis) is used to group the calculated trajectories based on its similarity of spatial distribution and number of optimal clusters considered based on the change in the spatial variance of all obtained trajectories (Draxler et al., 2014).

2.3 Uncertainties associated with the sensor and the reference laboratory to calibrate the instrument

In order to overcome the uncertainties associated with the collection of data by the sensor, some criteria were considered in this study as follows. First, in order to procure suitable multi-rotor components fitting the criteria of application, a detailed study was performed to choose the components offering the best performance and endurance for the flight plan of vertical profiling. Therefore, the frame dimension was chosen, which was capable of mounting the payload for vertical profiling. Besides, accurate decisions were made regarding (1) the BLDC motor KV rating providing enough torque and thrust to carry the payload, (2) the proper combination of propeller length and pitch offering good thrust to weight ratio and endurance, and (3) the LIPO (lithium polymer) battery rating providing the fly time required for the flight plan of vertical profiling.

Second, DJI NAZA M LITE was considered as the flight controller being used for the multi-rotor. Live data telemetry of parameters like altitude, battery status, live flight footage, and multi-rotor's orientation was required in this study to carry out the flight for data gathering. (1) A separate unit of FC was used to perform the telemetry. (2) The FC chosen was JHEMCU F7BT DUAL GYRO, since it had an inbuilt barometer and on-screen display (OSD). The barometer was used to get altitude data with the help of atmospheric pressure difference. (3) The camera and the VTX (video transmitter) were connected to the JHEMCU F7 flight controller and the data was received using a VRX (video receiver), which was connected to a monitor. (4) With the help of camera footage and OSD details on the monitor, the flight was performed.

Third, high wind current was one of the major uncertainty associated with the study. At an altitude of 40 m to 60 m the wind current was high resulting in an unsteady flight and rolling down of the multi-rotor. High wind currents lead to multiple crashes resulting in damage of the multi-rotor components like propellers and frame arms, leading to time-consuming delays to complete the study. Therefore, (1) flights were conducted considering the wind speed, certain flight maneuvers were performed to have a steady flight at high wind speeds; and (2) the flight controllers gain settings were tuned to offer high stability in windy situations.

Furthermore, the multi-rotor was built and calibrated by the Aerospace engineering department of Karunya Institute Of Technology And Sciences, and the following calibration procedure was considered for it. First, all the components were connected in a proper and correct way. Second, the transmitter was bound with the receiver. For the research, Radiomaster TX16s was bounded with a Flysky FSi6 receiver operating on 2.4 GHz, offering strong connectivity throughout the flight. Third, the ESC (Electronic Speed Controller) was calibrated, in which the maximum and minimum throttle values were given to the ESC, resulting in the spinning of all motors at the same RPM. And finally, the FC DJI NAZA M LITE was calibrated using the DJI NAZA configurator, which is a PC software.

3. Results and discussion

3.1 Data analysis

The distribution of the collected data for PM_1, $PM_{2.5}$, PM_{10}, CO_2, and HCHO in each of the five sampling locations are presented through Box and Whisker plots in Figure 2. The vertical lines in each plot (whiskers) show the minimum and maximum values, while the dots above the maximum or below the minimum points illustrate the outliers in the dataset. Besides, the boxes represent the lower and upper quartiles, with a line in the middle as the median. The mean for each plot is illustrated by an “X” sign.

Based on the plots in Figure 2, the collected data for different pollutants in this study is skewed, since the density of observations on the two sides of the median is not equal. Considering PM_1, $PM_{2.5}$, and PM_{10}, the Petrol Pump has the highest level of data density compared with the other locations, but on the other hand, it has the highest number of outliers. The Administration Block comes after the Petrol Pump in terms of both the density of the collected data and the number of outliers. In contrast with the Petrol Pump and the Administration Block, Bethesda’s data has the lowest density in terms of PM_1, $PM_{2.5}$, and PM_{10}, but it has no outlier. Except in the Petrol Pump, the range of observed values (between the minimum and maximum) in all the locations are the largest for PM_{10}. The second and third ranks go to $PM_{2.5}$ and PM_1, respectively. Besides, in all the five locations, PM_1, $PM_{2.5}$, and PM_{10} keep the same sequence if they are sorted based on the minimum, lower quartile, median, mean, upper quartile, or maximum (i.e. $PM_1 < PM_{2.5} < PM_{10}$ in terms of minimum, lower quartile, median, mean, upper quartile, and maximum in all the sampling locations). These sequences are clarified in Table 1.

As can be seen from the top right part of Figure 2, the collected CO_2 data in the Petrol Pump has a higher density in comparison with the other locations and is more concentrated between 408 and

459 ppm. Ignoring the two outliers, the range of data for this greenhouse gas in the Petrol Pump is lower in comparison with the other locations, with a minimum of 408 ppm and a maximum of 533 ppm. The collected data for CO_2 in the Flight Hangar is in contrast with the Petrol Pump since its range is larger (between 4.8 ppm as the minimum and 655 ppm as the maximum), and its density is lower (between 415 ppm as the first quartile and 515.5 ppm as the third quartile). The density of observations for HCHO, as illustrated in the bottom right of Figure 2, is the highest in the CTC Block (between 0.010 and 0.011 $mg\ /m^3$), followed by the Petrol Pump (between 0.009 and 0.011 $mg\ /m^3$). This is while the Administration Block, the Flight Hangar, and Bethesda are equally ranked third, having 0.009 and 0.012 $mg\ /m^3$ as their first and third quartiles. All these three locations have a minimum of 0.009 $mg\ /m^3$ in terms of HCHO concentration, which is equal to their first quartile. However, since the outliers are ignored, the maximum HCHO concentration in the Administration Block and the Flight Hangar are equal (both 0.016 $mg\ /m^3$), attributing to them the largest range of observed values. Bethesda is ranked second in this regard since its maximum value is 0.014 $mg\ /m^3$.

3.2 Impact of meteorological parameters and height on the concentration of pollutants in the sampling locations

Variations in the concentration of the pollutants evaluated in this study in the five locations at different sampling times indicate the influence of various parameters. The RH and temperature were measured in each trial at each of the four specified heights for sampling. Considering the variations observed between the sampling locations (Figure 2), we infer that some of the influential factors that are specific to each sampling location are not captured in our study. Therefore, here we analyze the role of RH, temperature, and height in different sampling locations on the concentration of pollutants.

In order to determine the most relevant factors for the concentration of pollutants, CHAID (CHi-square Automatic Interaction Detection) algorithm (Kass, 1980) was applied to build a Decision Tree (DT) for each of the pollutants. The DT is a data mining technique, which is trained on a base dataset and can identify the existing relationships between independent variables and the dependent variable (Hagenauer and Helbich, 2017) regardless of the linearity or non-linearity of the relationships (Gao et al., 2021). The DT is a tree-like model with several layers of node, in which the first node is the root, the terminal nodes are the leaves, and the internal nodes between the root and the leaves correspond to specific attributes. The CHAID algorithm applied to construct the DTs followed the steps of (a) merging, (b) splitting, and (c) stopping to derive statistically significant segments of data presented in non-binary tree-shaped models (Onwuegbuzie and Johnson, 2021). This algorithm uses Pearson’s chi-square test to best split the nodes at each step, and its procedure can be summarized as follows.

First, the categories of the independent variables are cross-tabulated with the categories of the dependent variable. Second, the pair of independent variable categories that have the least significant difference are identified and merged if the difference is less than a considered threshold. Third, the compound categories of independent variables are analyzed to identify the most statistically significant binary split if the significance exceeds the threshold. In case the split is done, the algorithm returns to the merging stage and repeats the merging and splitting stages. This repetition continues until all the merged categories of independent variables reach optimality.

Finally, the significance of all optimally merged variables is calculated (Kass, 1980; Rashidi et al., 2014; Huang and Lin, 2013).

To build the DTs in this research, the records containing missing or corrupted values were excluded from the database of the observations, and the remaining 2271 observations for each of the pollutants were used to build five DTs in IBM® SPSS® software, each for one of the measured pollutants. The role of the dependent variable was given to each of the pollutants in the DTs, whereas the other variables were considered as independent variables. To specify the importance level of *RH*, *temperature*, and *height* in the vertical concentration of pollutants in each sampling location, the variable "*location*" was forced to be used for branching at the first level in the DTs. Figures 3 to 6 illustrate the resulting CHAID DTs for PM_1, $PM_{2.5}$, PM_{10}, CO_2, and HCHO, respectively. As can be seen in these figures, all the branching processes in these DTs are highly statistically significant (P-value = 0.000). The mean and standard deviation mentioned in each node refers to the "n" observations located in that node.

The DT presented in Figure 3 shows that in the sampling locations Administration Block, Bethesda, and CTC Block, *RH* has the most important role in the concentration of PM_1. In these locations, when $RH \leq 48\%$, $RH > 71\%$, or $50\% < RH < 55\%$, *temperature* plays the second important role and *height* does not have any significant impact. On the contrary, when $55\% < RH < 57\%$ in these locations, *height* plays the second important role, and the *temperature* does not have any significant impact. For the ranges of 48%-50%, and 57%-61% for RH in the mentioned locations, neither *height* nor *temperature* play a significant role in the variations in the PM_1 concentration. Finally, for these three sampling locations, when $61\% < RH < 71\%$, regardless of *height* and *temperature*, we can separate Bethesda from the two other locations in terms of the mean of the observations located in that node. For the Petrol Pump, similar to the previously mentioned locations, *RH* has the most significant role. However, in this sampling location, neither *height* nor *temperature* proves to be significantly effective in PM_1 concentration. And last but not least, the branch referring to Flight Hangar identifies *temperature* as a significant player in terms of the changes in PM_1 concentration and removes *RH* and *height* from the list of significantly effective factors in this location.

Considering *location* as the branching variable in the first level in Figure 4, Petrol Pump grasps a separate node from the other locations, which are in the same node altogether. In the Petrol Pump, *temperature* is the leading factor in terms of the $PM_{2.5}$ concentration, and only if *temperature* is between 84.6 °F and 85.1 °F (or equivalently, $29.22\,°\mathrm{C} < temperature < 29.5\,°\mathrm{C}$), *RH* is considered the next significantly effective factor. In the other four sampling locations, *RH* is identified as the most significantly effective factor in the concentration of $PM_{2.5}$. When $RH \leq 43\%$, $RH > 71\%$, or $48\% < RH < 55\%$, *temperature* is the next significantly effective factor, while if $55\% < RH < 57\%$, *height* plays the next important role. Finally, when $43\% < RH < 47\%$ *or* $61\% < RH < 71\%$, the observations are split again based on *location*.

When it comes to PM_{10}, the sampling locations are put into three nodes in the first level of branching in the DT, as illustrated in Figure 5. In the Petrol Pump, *temperature* has the most statistically significant impact on the concentration of PM_{10}, followed by *height*, as the next significant factor. Similar to the Petrol Pump, in the Administration Block and Flight Hangar, the main branches are made based on *temperature*. However, in the next level, *RH* is the leading factor for the observations made in the *temperature* between 82.1 °F and 84.2 °F (or equivalently, $27.83\,°\mathrm{C} < temperature < 29\,°\mathrm{C}$), and *location* becomes important for the observations made in the *temperature* between 84.2 °F and 85.1 °F (or equivalently, $29\,°\mathrm{C} < temperature < 29.5\,°\mathrm{C}$). Finally, the branching for Bethesda and CTC Block is based on *RH*, followed by *temperature* when $RH \leq 48\%$, $RH > 71\%$, or $50\% < RH < 51\%$, and by *location* when $61\% < RH < 71\%$.

Figure 6 shows more splits based on the *location* when analyzing the concentration of CO_2. Although *RH* is the main significant effective factor on the concentration of CO_2, for Administration Block, CTC Block, Bethesda, and Petrol Pump, the second effective factor is different for various ranges of *RH*. In the Administration Block and CTC Block, for $RH > 61\%$, *height* is the next effective factor, while for $50\% < RH < 57\%$, *temperature* plays the next significant role. For other ranges of *RH* values, no significant factor is identified. In Bethesda, when $61\% < RH < 71\%$, no other significant factor is identified, while if $RH \leq 61\%$, *height* is identified as the second significantly effective factor and if $RH > 71\%$, *temperature* plays an effective role in determining the concentration of CO_2. In the Petrol Pump, after *RH*, *height* is identified as a significantly effective factor, but only when $48\% < RH < 57\%$. The case is different in Flight Hangar, as *temperature* is the leading factor in splitting the observations, and *RH* is the second significantly effective factor only for the observations referring to the *temperature* between 79.4 and 85.1 °F (or equivalently, between 26.33 °C and 29.5 °C).

The CHAID DT in Figure 7 makes a separation between Petrol Pump and the other sampling locations by considering only two nodes in the first level of branching. In Petrol Pump, *temperature* has been identified as a statistically significant variable to split the observations on the concentration of HCHO. However, for all the other sampling locations, *RH* is the main identified significant factor that makes the splits in the next level of branching. In case $43\% <$

$RH < 47\%$, $53\% < RH < 57\%$, or $RH > 71\%$, *height* would be the second significantly effective factor in terms of the concentration of HCHO. For the observations with $48\% < RH < 53\%$ and $57\% < RH < 71\%$, the second split of observations would be based on *location*. For other ranges of *RH*, no factor is recognized as to be statistically significant.

We show in Figure 2 a general view of the differences between the observations in each location. Figures 3 to 7 illustrate a more in-depth analysis of the role of location along with the meteorological parameters and height on the concentration of pollutants. The analysis presented in this section confirms the findings from the initial statistical analysis, highlighting that in addition to the meteorological parameters and height, different attributes of the sampling locations may affect the concentration of studied pollutants. These attributes may be linked with the width of the sampling location, the height of the nearby buildings, wind direction, or other factors. However, a detailed analysis of the location attributes is out of the scope of this research, and therefore we provide an analysis of the concentration of pollutants with respect to meteorological parameters and height.

3.3 The concentration of pollutants with respect to meteorological parameters and height

In order to better visualize the changes in the concentration of the studied pollutants with respect to the meteorological parameters and height, a fuzzified DT-based 4-D space is developed for each of the pollutants, and then, the 3-D surfaces extracted from these spaces are presented in this section. To do so, two main steps were taken.

First, the recorded observations for each of the pollutants were introduced into a DT with the CHAID growing method to build five new decision trees based on the observations related to the pollutants, this time regardless of their sampling location. The overall accuracy of the DTs was confirmed by their risk estimate (within-node variance). The risk estimate for PM_1, $PM_{2.5}$, PM_{10}, CO_2, and HCHO was 60.35, 90.727, 221.557, 1123.556, and 1.469E-6, respectively. Considering the structure of the DTs, relevant if-then rules were extracted for each leaf, such as "$IF\ [(RH \leq 43))\ and\ (TEMP > 85.09))]\ THEN\ [PM1\ Prediction = 30.37]$". The predicted values for the pollutants in each node of the tree refer to the mean of the observations located in that node.

Second, based on the ranges of values determined by the branches of the DTs, relevant membership functions were designed for the pollutants, height, RH, and temperature to build a Fuzzy Inference System (FIS) in MATLAB® for each of the pollutants. All these membership functions were set in the form of Gaussian functions. Furthermore, the rules extracted from each DT were used to build the Mamdani rule-based inference engine for the FISs.

The built FISs can be used to estimate the concentration of pollutants with respect to different levels of RH, temperature, and height (Ranjbari et al., 2021). However, since this is not the main purpose of our study, we have only applied them to visualize the relationship between various levels of meteorological parameters and the pollutants through 3-D surfaces.

Figures 8 to 10 show the changes in the concentration of the studied pollutants with respect to *RH* and *temperature*, *height* and *temperature*, and *RH* and *height*, respectively. Each variable follows its own scale in these figures, and a color range of dark blue to bright yellow is used to show very low to very high concentrations of studied pollutants based on their own scale of measurement.

Figure 8 provides a general view of the concentration of the pollutants, considering *RH* and *temperature*. As can be seen from this figure, the concentration of each of the pollutants has different behavior in terms of the changes in *RH* and *temperature*. However, the surfaces referring to PM_1, $PM_{2.5}$, and PM_{10} follow the same behavior in some points. For these three pollutants, high levels of *RH* and *temperature* leads to low concertation of the pollutants. Besides, PM_1 and $PM_{2.5}$ show rather similar fluctuations in most parts of the surface. Focusing on the fluctuations caused by the changes in the values in X and Y axes, it can be inferred that changes in the *RH* have a stronger effect than *temperature* in changing the concentration of PM_1, $PM_{2.5}$, PM_{10}, and CO_2. However, this cannot be concluded for HCHO, since both variables seem to be effective in making the changes in the HCHO concentration.

Having an overview of the surfaces presented in Figure 9, it can be seen that compared with *temperature*, *height* has a very weak role in changing the concentration levels of PM_1, $PM_{2.5}$, PM_{10}, and CO_2. Besides, considerable changes due to *temperature* start to occur when the *temperature* exceeds 80 °F, leading to an increased concentration of PM_1, $PM_{2.5}$, and CO_2 and decreasing PM_{10}. Again, HCHO concentration shows a different behavior compared with the other pollutants and is slightly affected by both of the considered factors.

Referring to Figure 10, the stronger impact of *RH* changes compared with the *height* changes on the concentration of PM_1, $PM_{2.5}$, PM_{10}, and CO_2 is realizable. As can be seen in this figure, the concentration of PM_1, $PM_{2.5}$, and PM_{10} have almost similar fluctuations after around 55% of *RH* regardless of the height, but with different levels of pollutant concentration. Besides, considerable fluctuations are observed due to changes in the *RH* level, which highlight the significant role of *RH* in pollutant concentrations. These fluctuations were also observed in Figure 8 when comparing the significance of changes made by *RH* and *temperature*. Similar to the previous figures in this section, different behavior is observed in the HCHO surface, indicating more impact received from *height*, in comparison with the other pollutants. These analyses also confirm the strong role of *RH* and the weak role of *height*, in comparison with other factors, regarding the concentration of the studied pollutants.

3.4 Cluster analysis

This section reports the results of cluster analysis to evaluate the contribution of possible sources of aerosols from different regions. Figure 11 shows the clusters of five days air mass back trajectories arriving at the observation site from different regions. Air mass back trajectories were calculated using the HYSPLIT model and it is used for the indication of general airflow followed by an air parcel. Further, these trajectories were merged together representing a group called a cluster. Differences between trajectories within the clusters are minimized and the difference between clusters is maximized.

The distributions of four clusters were calculated for the hourly airmass trajectories clusters obtained for each day of the observation period. The highest number of trajectories belongs to cluster 2 (41%) arriving from the Bay of Bengal region. Cluster 1 (39%) and cluster 4 (17%) contribute significantly to the air mass arriving at the observation site during the observation period. All these trajectories carry the effect of air mass originating from the Bay of Bengal with a longer range for cluster 4 from the altitude range up to 2000 m AGL, as indicated in the vertical profile of airmass with distance from the observation site in Figure 11. The other clusters (except cluster 2) achieve altitudes lower than 500 m AGL only for all hours of observation before reaching the observation site. The lowest contribution of air mass is obtained from trajectories corresponding to cluster 3 (3%) originating from the Arabian sea region. Clusters highlight the pathways of air mass and advected moisture from oceanic regions adjacent to the observation site.

Vertical columns in the lower section of figure 11 indicate the percentage contribution of each cluster to the individual day of the observation period.

The contribution of each cluster to individual days is presented by the corresponding colors of the respective cluster. It is observed that trajectories corresponding to cluster 2 contributed to almost all days and cluster 1 contains trajectories of days except 09-12 March. Air mass corresponding to cluster 3 arrives at the observation site on 06 and 07 March only, with the lowest number of trajectories corresponding to it. Nair et al. (2008) characterized the influence of marine aerosols originating from the Arabian Sea and Bay of Bengal reaching over the Indian subcontinent. It contains the aerosols dominated by SO_4^{2-}, NH_4^+, and NO_3^- over the oceanic region, and suggests the presence of ammonium sulfate and ammonium nitrate which are responsible for the radiation budget in the atmosphere.

4. Summary and conclusion

This study presents the vertical distribution of air pollutants based on the measurements conducted by UAV at different fixed locations in a rural area of southern India. The investigations were carried out through 30 flights in March 2021 to gather data regarding the concentration of PM_{10}, $PM_{2.5}$, PM_1, CO_2, and HCHO as well as RH and temperature in four height levels (15, 30, 45, and 60 m) in five different locations within the area of Karunya Institute of Technology and Sciences, Karunya Nagar, Coimbatore.

The gathered database was used to build a CHAID DT for each of the pollutants, considering different sampling locations for the analysis. The results indicate the weak role of height on the concentration of pollutants in the sampling locations, and instead, highlight the role of temperature and RH in this regard. Besides, to better visualize the relationship between the concentration of each of the studied pollutants and height, RH, and temperature regardless of the specific sampling locations, new CHAID DTs were built for the pollutants, disregarding the sampling locations, and the extracted "if-then" rules were used to build fuzzy surfaces for each pollutant. These surfaces show that in comparison with the other studied pollutants, HCHO is more variant with the changes in height, and the concentration of HCHO changes more than the other pollutants by changing height and the RH level. The findings are then confirmed by the cluster analysis, which showed that meteorological parameters, regional transport, and atmospheric condition may play an essential role in the vertical distribution of air pollutants.

The study area of Karunya Nagar is located in the southernmost part of the Indian peninsula and the prevailing air masses exert more influence on the concentration profile of air pollutants with different sources than inland cities. The significant impact of regional transport/ sources was analyzed using cluster analysis (back- trajectory). Cluster analysis of five days' hourly air mass back-trajectories suggests the contribution of possible sources of air mass transported over the observation site. The maximum contribution of air mass is from the Bay of Bengal, which contributes to the loading of pollutant concentration over a different altitude of India's rural area. Furthermore, the relationship between the vertical concentration of pollutants and meteorological parameters was observed by advanced statistical analysis. The outcomes of the study indicate the potential of identifying the vertical distribution of air pollutants by using UAV measurements. Besides, it can be realized from this study that transport, through both advection and convection, influences the vertical distribution of air pollutants as inferred from meteorological analysis, including back trajectories using the Hybrid Single-Particle Lagrangian Integrated Trajectory (HYSPLIT4) model. The long-range transport of air mass could also contribute to the high concentration values of particulate matters, as found through the five-day air mass backward trajectory analysis. Although the observed data sets are confined to a height of 60 m AGL, the results from this study provide insights into the vertical distribution of air pollutants, complementing ground-based measurement variations with different spacing and timing.

However, further studies are suggested to clarify the different times (other times of the day), space/locations, and extended altitudes to gain insights into the vertical profile/movement of air pollutants upward.

Acknowledgments

We are thankful to Karunya Institute of Technology and Sciences Coimbatore, Tamil Nadu, India for providing us the required funding to complete this study.

References

Allaby, M., 2007. Encyclopedia of Weather and Climate. Rev. Facts on File (Facts on File science library, New York (2007). [Last Assess:13 July, 2021].

Argyropoulos, G., Grigoratos, T., Voutsinas, M., Samara, C., 2013. Concentrations and source apportionment of PM10 and associated elemental and ionic species in a lignite-burning power generation area of southern Greece. Environ. Sci. Pollut. Rea. 20, 7214 – 7230.

Bates, T.S., Quinn, P.K., Johnson, J.E., Corless, A., Brechtel, F.J., Stalin, S.E., Meinig, C., Burkhart, J.F., 2013. Measurements of atmospheric aerosol vertical distributions above Svalbard, Norway, using unmanned aerial systems (UAS). Atmos. Meas. Tech. 6, 2115 – 2120. https://doi.org/10.5194/amt - 6 -2115 -2013

Baumbach, G., Vogt. U., 2003. Influence of inversion layers on the distribution of air pollutants in urban areas. Water Air Soil Pollut. 3 (5–6), 65-76.

Borbély-Kiss, I., Koltay, E., Szabó, G.Y., Bozó, L., Tar, K., 1999. Composition and sources of urban and rural atmospheric aerosol in eastern Hungary. J. Aero. Sci. 30, 369 – 391.

Bond, T.C., Doherty, S.J., Fahey, D.W., Forster, P.M., Berntsen, T., Deangelo, B.J., Flanner, M.G., Ghan, S., Kärcher, B., Koch, D., Kinne, S., Kondo, Y., Quinn, P.K., Sarofim, M.C., Schultz, M.G., Schulz, M., Venkataraman, C., Zhang, H., Zhang, S., Bellouin, N., Guttikunda, S.K., Hopke, P.K., Jacobson, M.Z., Kaiser, J.W., Klimont, Z., Lohmann, U., Schwarz, J.P., Shindell, D., Storelvmo, T., Warren, S.G., Zender, C.S., 2013. Bounding the role of black carbon in the climate system: A scientific assessment. J. Geophys. Res. Atmos. 118, 5380 –5552. https://doi.org/10.1002/jgrd.50171

Chilinski, M.T., Markowicz, K.M., Markowicz, J., 2016. Observation of vertical variability of black carbon concentration in lower troposphere on campaigns in Poland. Atmos. Environ. 137, 155 –170. https://doi.org/10.1016/j.atmosenv.2016.04.020

Ding, A., Wang, T., Xue, L., Gao, J., Stohl, A., Lei, H., Jin, D., Ren, Y., Wang, X., Wei, X., Qi, Y., Liu, J., Zhang, X., 2009. Transport of north China air pollution by midlatitude cyclones: Case study of aircraft measurements in summer 2007. J. Geophys. Res. Atmos. 114, 1 –16. https://doi.org/10.1029/2008JD011023

Draxler, R., Stunder, B., Rolph, G., Stein, A., Taylor, A., 2014. HYSPLIT4 user's guide version 4 - Last revision: September 2014.

Essa, K.S.M., Mubarak, F., Elsaid, S.E.M., 2006. Effect of the plume rise and wind speed on extreme value of air pollutant concentration. Meteorol. Atmos. Phys. https://doi.org/10.1007/s00703 -005 -0168 - 1

Ferrero, L., Mocnik, G., Ferrini, B.S., Perrone, M.G., Sangiorgi, G., Bolzacchini, E., 2011. Vertical profiles of aerosol absorption coefficient from micro -Aethalometer data and Mie calculation over Milan. Sci. Total Environ. 409, 2824 –2837. https://doi.org/10.1016/j.scitotenv.2011.04.022

Ferrero, L., Perrone, M.G., Petraccone, S., Sangiorgi, G., Ferrini, B.S., Lo Porto, C., Lazzati, Z., Cocchi, D., Bruno, F., Greco, F., Riccio, A., Bolzacchini, E., 2010. Vertically - resolved particle size distribution within and above the mixing layer over the Milan metropolitan area. Atmos. Chem. Phys. https://doi.org/10.5194/acp -10 -3915 -2010

Gao, Y., Wang, Z., Li, C.Y., Zheng, T. and Peng, Z.R., 2021. Assessing neighborhood variations in ozone and PM2. 5 concentrations using decision tree method. Building and Environment, 188, p.107479.

Gautam, S., Kumar, P., Patra, A.K., 2016. Occupational exposure to particulate matter in three Indian opencast mines. Air Qual. Atmos. Health 9(2), 143-158.

Gautam, S., Patra, A.K., 2015. Dispersion of particulate matter generated at higher depths in opencast mines Environ.Technol. Inn. 3, 11-27.

Gollakota, A.R.K., Gautam, S., Santosh, M., Sudan, H.A., Gandhi, R., Jebadurai, V.S., Shu, CM., 2021. Bioaerosols: characterization, pathways, sampling strategies, and challenges to geo-environment and health. Gondwana Research 99, 178-203, doi.org/10.1016/j.gr.2021.07.003.

Günter Baumbach. Air Quality Control. Formation and Sources, Dispersion, Characteristics and Impact of Air Pollutants? Measuring Methods, Techniques for Reduction of Emissions and Regulations for Air Quality Control. Springer Berlin Heidelberg (Environmental Engineering), Berlin, Heidelberg (1996).

Guzmán-Torres, D., Eiguren-Fernández, A., Cicero-Fernández, P., Maubert-Franco, M., Retama-Hernández, A., Villegas, R., Rafael, Miguel, A. H., 2009. Effects of meteorology on diurnal and nocturnal levels of priority polycyclic aromatic hydrocarbons and elemental and organic carbon in PM10 at a source and a receptor area in Mexico City. Atmos. Environ. 43 (17), 2693-2699.

Hagenauer, J. and Helbich, M., 2017. A comparative study of machine learning classifiers for modeling travel mode choice. Expert Systems with Applications, 78, pp.273-282.

Han, S., Zhang, Y., Wu, J., Zhang, X., Tian, Y., Wang, Y., Ding, J., Yan, W., Bi, X., Shi, G., Cai, Z., Yao, Q., Huang, H., Feng, Y., 2015. Evaluation of regional background particulate matter concentration based on vertical distribution characteristics. Atmos. Chem. Phys. 15, 11165 –11177. https://doi.org/10.5194/acp -15 -11165 -2015

Huang, C. and Lin, Y., 2013. "Applying CHAID algorithm to investigate critical attributes of void formation in QFN assembly", Soldering & Surface Mount Technology, Vol. 25 No. 2, pp. 117-127. https://doi.org/10.1108/09540911311309086Janhall, S., Olofson, K., Andersson, P., Pettersson, J., Hallquist, M., 2006. Evolution of the urban aerosol during winter temperature inversion episodes. Atmos. Environ. 40 (28), 5355-5366.

Kass, G.V., 1980. An exploratory technique for investigating large quantities of categorical data. Journal of the Royal Statistical Society: Series C (Applied Statistics), 29(2), pp.119-127.

Klompmaker, J.O., Montagne, D.R., Meliefste, K., Hoek, G., Brunekreef, B., 2015. Spatial variation of ultrafine particles and black carbon in two cities: Results from a short -term measurement campaign. Sci. Total Environ. 508, 266 –275. https://doi.org/10.1016/j.scitotenv.2014.11.088

Lee, M., Brauer, M., Wong, P., Tang, R., Tsui, T.H., Choi, C., Cheng, W., Lai, P.C., Tian, L., Thach, T.Q., Allen, R., Barratt, B., 2017. Land use regression modelling of air pollution in high density high rise cities: A case study in Hong Kong. Sci. Total Environ. https://doi.org/10.1016/j.scitotenv.2017.03.094

Lei, X., Xiu, G., Li, B., Zhang, K., Zhao, M., 2016. Individual exposure of graduate students to PM2.5 and black carbon in Shanghai, China. Environ. Sci. Pollut. Res. 23, 12120 – 12127. https://doi.org/10.1007/s11356 -016 -6422 - x

Li, Y.J., Lee, B.P., Su, L., Fung, J.C.H., Chan, C.K., 2015. Seasonal characteristics of fine particulate matter (PM) based on high -resolution time -of-flight aerosol mass spectrometric (HR -ToF -AMS) measurements at the HKUST Supersite in Hong Kong.Atmos. Chem. Phys. 15, 37 –53. https://doi.org/10.5194/acp -15 -37 -2015

Liu, B., He, M.M., Wu, C., Li, J., Li, Y., Lau, N.T., Yu, J.Z., Lau, A.K.H., Fung, J.C.H., Hoi, K.I., Mok, K.M., Chan, C.K., Li, Y.J., 2019. Potential exposure to fine particulate matter (PM2.5) and black carbon on jogging trails in Macau. Atmos. Environ. 198, 23 – 33. https://doi.org/10.1016/j.atmosenv.2018.10.024

Lu, Y., Zhu, B., Huang, Y., Shi, S., Wang, H., An, J., Yu, X., 2019. Vertical distributions of black carbon aerosols over rural areas of the Yangtze River Delta in winter. Sci. Total Environ. https://doi.org/10.1016/j.scitotenv.2019.01.170

Minguillón, M.C., Brines, M., Pérez, N., Reche, C., Pandolfi, M., Fonseca, A.S., Amato, F., Alastuey, A., Lyasota, A., Codina, B., Lee, H.K., Eun, H.R., Ahn, K.H., Querol, X., 2015. New particle formation at ground level and in the vertical column over the Barcelona area. Atmos. Res. 164 –165, 118 –130. https://doi.org/10.1016/j.atmosres.2015.05.003

Mijling, B., Van Der, R. J., 2012. Using daily satellite observations to estimate emissions of short-lived air pollutants on a mesoscopic scale. J. Geophys. Rea. Atmos. 117, D17302.

Moreno-Ríos, A.L., Tejeda-Benitez, L. and Bustillo-Lecompte, C., 2021. Sources, characteristics, toxicity, and control of ultrafine particles: An overview. Geoscience Frontiers, p.101147.

Nair, V.S., Babu, S.S., Moorthy, K.K., 2008. Aerosol characteristics in the marine atmospheric boundary layer over the Bay of Bengal and Arabian Sea during ICARB: Spatial distribution and latitudinal and longitudinal gradients. Journal of Geophysical Research –Atmosphere, 10.1029/2008JD009823.

Olofson, K.F.G., Andersson, U. P., Hallquist, M., Ljungström, E., Tang, L., Chen, D., Pettersson, J.B.C., 2009. Urban aerosol evolution and particle formation during wintertime temperature inversions. Atmos. Environ. 43 (2),340-346.

Onwuegbuzie, A.J. and Johnson, R.B. eds., 2021. The Routledge Reviewer’s Guide to Mixed Methods Analysis. Routledge.

Panday, A. K., Prinn. R. G., 2009. Diurnal cycle of air pollution in the kathmandu valley, Nepal: observations. J. Geophys. Res., 114 (D9). 1295.

Patra, A.K., Gautam, S., Majumdar, S., Kumar, P., 2016. Prediction of particulate matter concentration profile in an opencast copper mine in India using an artificial neural network model. Air Qual. Atmos. Health 9 (6), 697–711. (IF = 2.87)

Peng, Z.R., Wang, D., Wang, Z., Gao, Y., Lu, S., 2015. A study of vertical distribution patterns of PM2.5 concentrations based on ambient monitoring with unmanned aerial vehicles: A case in Hangzhou, China. Atmos. Environ. 123, 357 –369. https://doi.org/10.1016/j.atmosenv.2015.10.074

Philip, S., Eric L., 2007. Vawdrey, Misty Corbett, Mark Erupe. Fine particle concentrations and composition during wintertime inversions in Logan, Utah, USA. Atmos. Environ. 41 (26), 5410-5422.

Praveen, P.S., Ahmed, T., Kar, A., Rehman, I.H., Ramanathan, V., 2012. Link between local scale BC emissions in the Indo -Gangetic plains and large scale atmospheric solar absorption. Atmos. Chem. Phys. 12, 1173 –1187. https://doi.org/10.5194/acp -12 -1173 - 2012

Ran, L., Deng, Z., Xu, X., Yan, P., Lin, W., Wang, Y., Tian, P., Wang, P., Pan, W., Lu, D., 2016. Vertical profiles of black carbon measured by a micro -aethalometer in summer in the North China Plain. Atmos. Chem. Phys. 16, 10441 –10454. https://doi.org/10.5194/acp -16 -10441 -2016

Ranjbari, M., Shams Esfandabadi, Z., Scagnelli, S. D., Siebers, P.-O., & Quatraro, F. (2021). Recovery agenda for sustainable development post COVID-19 at the country level: developing a fuzzy action priority surface. *Environment, Development and Sustainability*, *0123456789*. https://doi.org/10.1007/s10668-021-01372-6

Rashidi, S., Ranjitkar, P. and Hadas, Y., 2014. Modeling bus dwell time with decision tree-based methods. Transportation Research Record, 2418(1), pp.74-83.

Ravina, M., Shams Esfandabadi, Z., Panepinto, D., Zanetti, M.C., 2021. Traffic-induced atmospheric pollution during the COVID-19 lockdown: Dispersion modeling based on traffic flow monitoring in Turin, Italy. J. Clean. Prod. https://doi.org/10.1016/j.jclepro.2021.128425

Retama, A., Baumgardner, D., Raga, G.B., McMeeking, G.R., Walker, J.W., 2015. Seasonal and diurnal trends in black carbon properties and co -pollutants in Mexico City. Atmos. Chem. Phys. 15, 9693 –9709. https://doi.org/10.5194/acp -15 -9693 -2015

Samad, A., Vogt, U., Panta, A., & Uprety, D., 2020. Vertical distribution of particulate matter, black carbon and ultra-fine particles in Stuttgart, Germany. Atmos. Pollut. Res. 11(8), 1441–1450.

Schuyler, T., Guzman, M., 2017. Unmanned Aerial Systems for Monitoring Trace Tropospheric Gases. Atmosphere (Basel). 8, 206. https://doi.org/10.3390/atmos8100206

Silva, L.F., Santosh, M., Schindler, M., Gasparotto, J., Dotto, G.L., Oliveira, M.L. and Hochella Jr, M.F., 2021. Nanoparticles in fossil and mineral fuel sectors and their impact on environment and human health: A review and perspective. Gondwana Research 92, 184-201.

Stein, A.F., Draxler, R.R., Rolph, G.D., Stunder, B.J.B., Cohen, M.D., Ngan, F., 2015. Noaa's hysplit atmospheric transport and dispersion modeling system. Bull. Am. Meteorol. Soc. 96, 2059 –2077. https://doi.org/10.1175/BAMS - D -14 -00110.1

Strawbridge, K.B., Snyder, B.J., 2004. Daytime and nighttime aircraft lidar measurements showing evidence of particulate matter transport into the Northeastern valleys of the Lower Fraser Valley, BC. Atmos. Environ. 38, 5873 –5886. https://doi.org/10.1016/j.atmosenv.2003.10.036

Tang, G., Zhang, Jinqiang, Zhu, X., Song, T., Münkel, C., Hu, B., Schäfer, K., Liu, Z., Zhang, Junke, Wang, L., Xin, J., Suppan, P., Wang, Y., 2016. Mixing layer height and its implications for air pollution over Beijing, China. Atmos. Chem. Phys. 16, 2459 –2475. https://doi.org/10.5194/acp -16 -2459 -2016

Vardoulakis, S., Giagloglou, E, et al., 2020. Indoor exposure to selected air pollutants in the home environment: A systematic review. International Journal of Environmental Research and Public Health 17, 8972.

Villa, T., Salimi, F., Morton, K., Morawska, L., Gonzalez, F., 2016. Development and Validation of a UAV Based System for Air Pollution Measurements. Sensors 16, 2202. https://doi.org/10.3390/s1612220 2

Wang, Y.Q., Zhang, X.Y., Sun, J.Y., Zhang, X.C., Che, H.Z., Li, Y., 2015. Spatial and temporal variations of the concentrations of PM 10 , PM 2.5 and PM 1 in China. Atmos. Chem. Phys. Discuss. 15, 15319 –15354. https://doi.org/10.5194/acpd -15 -15319 -2015

Zoras, S., Triantafyllou, A.G., Deligiorgi, D., 2006. Atmospheric stability and PM10 concentrations at far distance from elevated point sources in complex terrain: worst-case episode study. J. Environ. Manag. 80 (4), 295-302.

Zhou, S., Peng, S., Wang, M., Shen, A., Liu, Z., 2018. The Characteristics and Contributing Factors of Air Pollution in Nanjing: A Case Study Based on an Unmanned Aerial Vehicle

Experiment and Multiple Datasets. Atmosphere (Basel). 9, 343. https://doi.org/10.3390/atmos9090343.

Figure captions

Figure 1: Location of Karunya Nagar, Karunya Institute of Technology and Sciences in the Tamil Nadu State of southern India (red circle within map of India), with the flight site and the meteorological station.

Figure 2. Box and Whisker plots for graphic presentation of the collected data for PM_1, $PM_{2.5}$, PM_{10}, CO_2, and HCHO in each of the five sampling locations

Figure 3. The overall structure of the CHAID DT for PM_1. Locations are as follows. A: Administration Block; B: Bethesda; C: CTC Block; F: Flight Hangar; P: Petrol Pump.

Figure 4. The overall structure of the CHAID DT for $PM_{2.5}$. Locations are as follows. A: Administration Block; B: Bethesda; C: CTC Block; F: Flight Hangar; P: Petrol Pump.

Figure 5. The overall structure of the CHAID DT for PM_{10}. Locations are as follows. A: Administration Block; B: Bethesda; C: CTC Block; F: Flight Hangar; P: Petrol Pump.

Figure 6. The overall structure of the CHAID DT for CO_2. Locations are as follows. A: Administration Block; B: Bethesda; C: CTC Block; F: Flight Hangar; P: Petrol Pump.

Figure 7. The overall structure of the CHAID DT for HCHO. Locations are as follows.: A: Administration Block; B: Bethesda; C: CTC Block; F: Flight Hangar; P: Petrol Pump.

Figure 8. The concentration of pollutants based on *temperature* and *RH.*

Figure 9. The concentration of pollutants based on temperature and height.

Figure 10. The concentration of pollutants based on *RH* and *height.*

Figure 11. Cluster analysis of five days' hourly air mass back-trajectories arriving at 500 m AGL over the observation site.

Table captions

Table 1. The sequence of PM_1, $PM_{2.5}$, and PM_{10} concentration in the studied locations in terms of the minimum, lower quartile, mean, upper quartile, and maximum

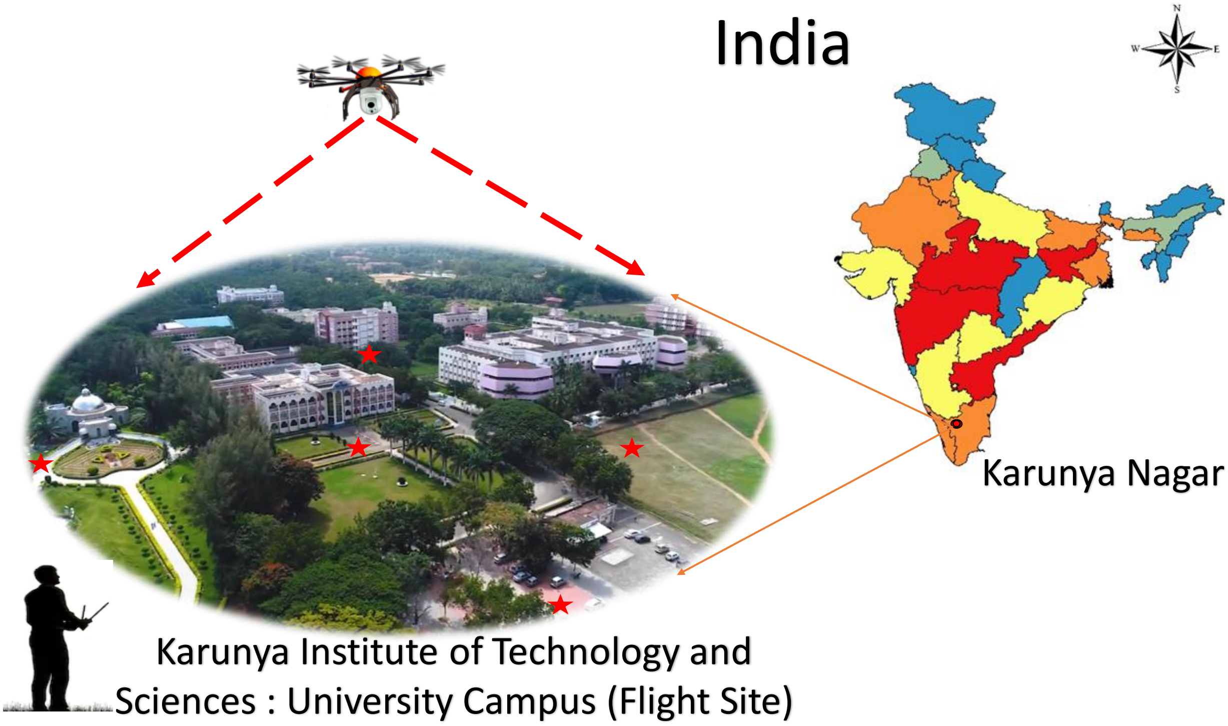

Figure 1: Location of Karunya Nagar, India. Karunya Institute of Technology and Sciences with the flight site and the meteorological station is denoted using a red dot in the picture at the lower-left portion of the figure.

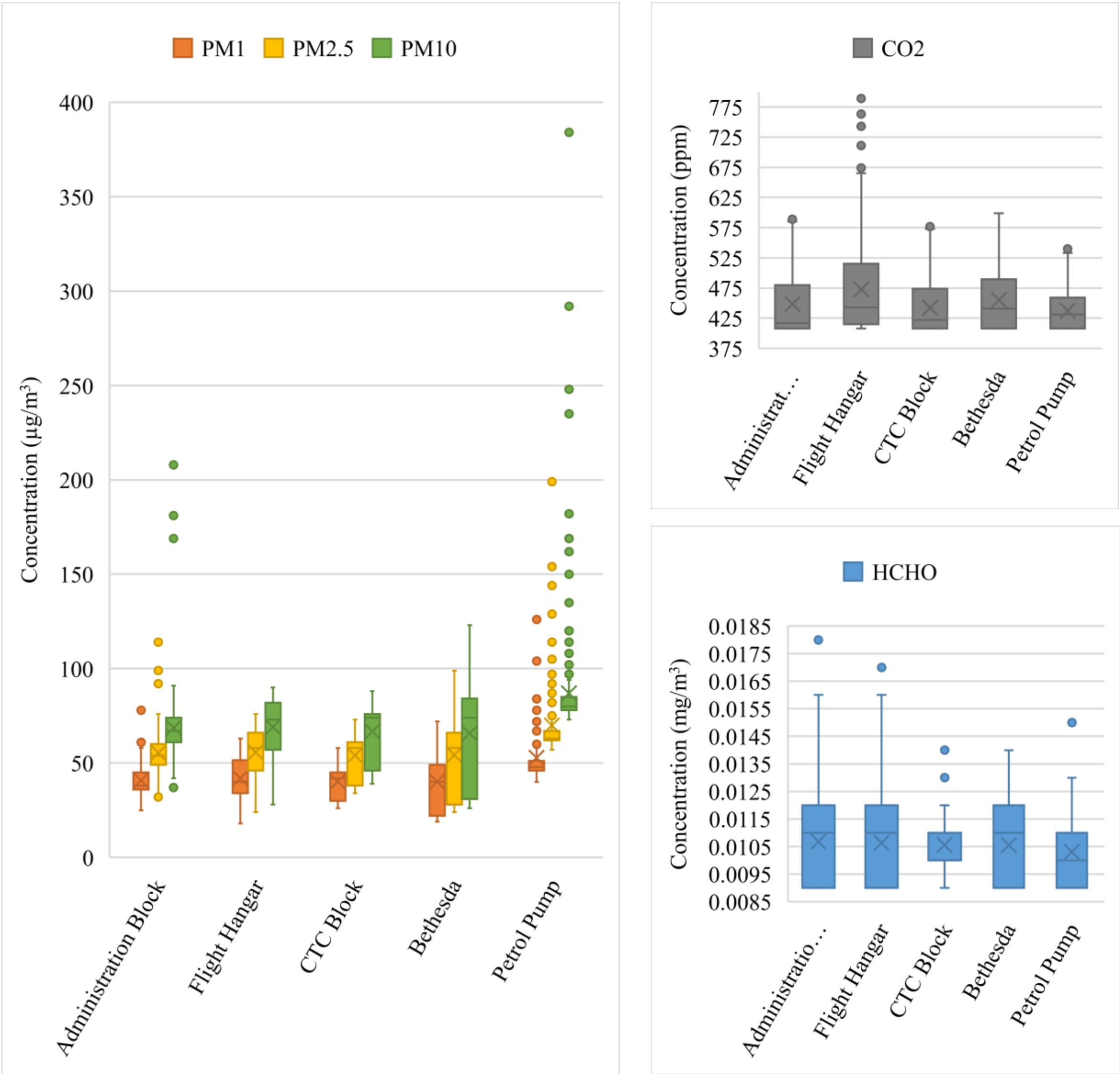

Figure 2. Box and Whisker plots for graphic presentation of the collected data for PM_1, $PM_{2.5}$, PM_{10}, CO_2, and HCHO in each of the five sampling locations

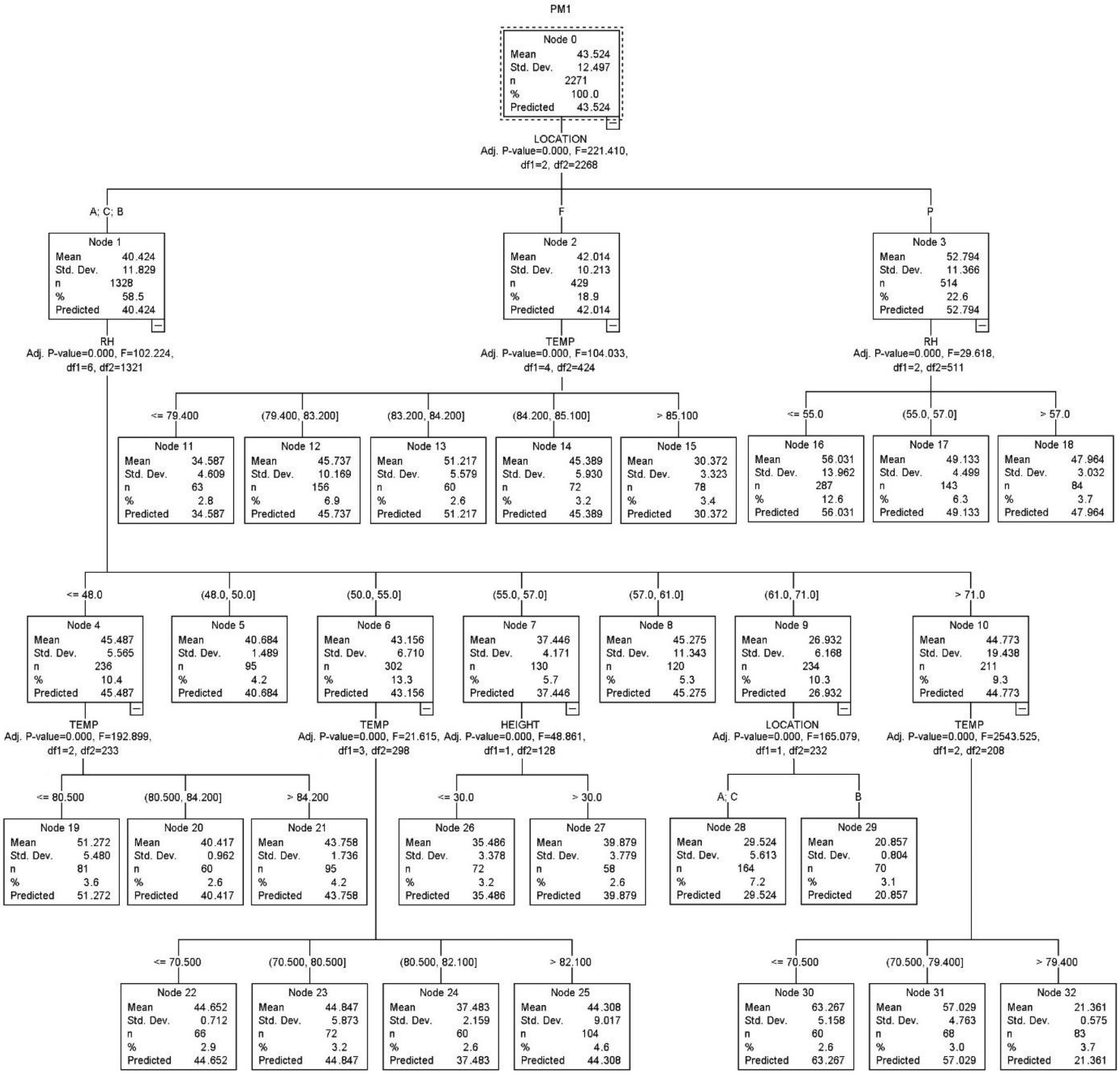

Figure 3. The overall structure of the CHAID DT for PM_1

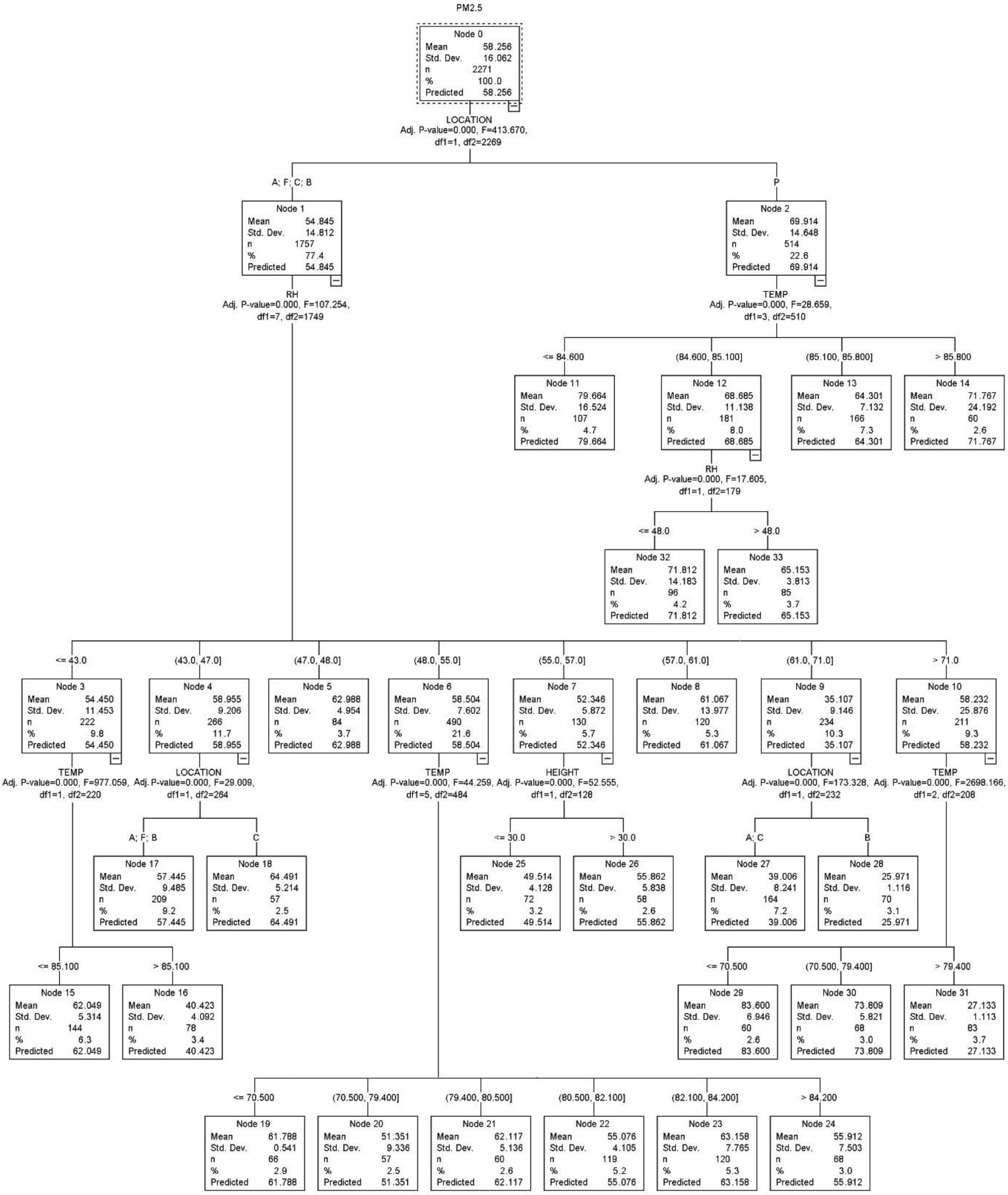

Figure 4. The overall structure of the CHAID DT for $PM_{2.5}$

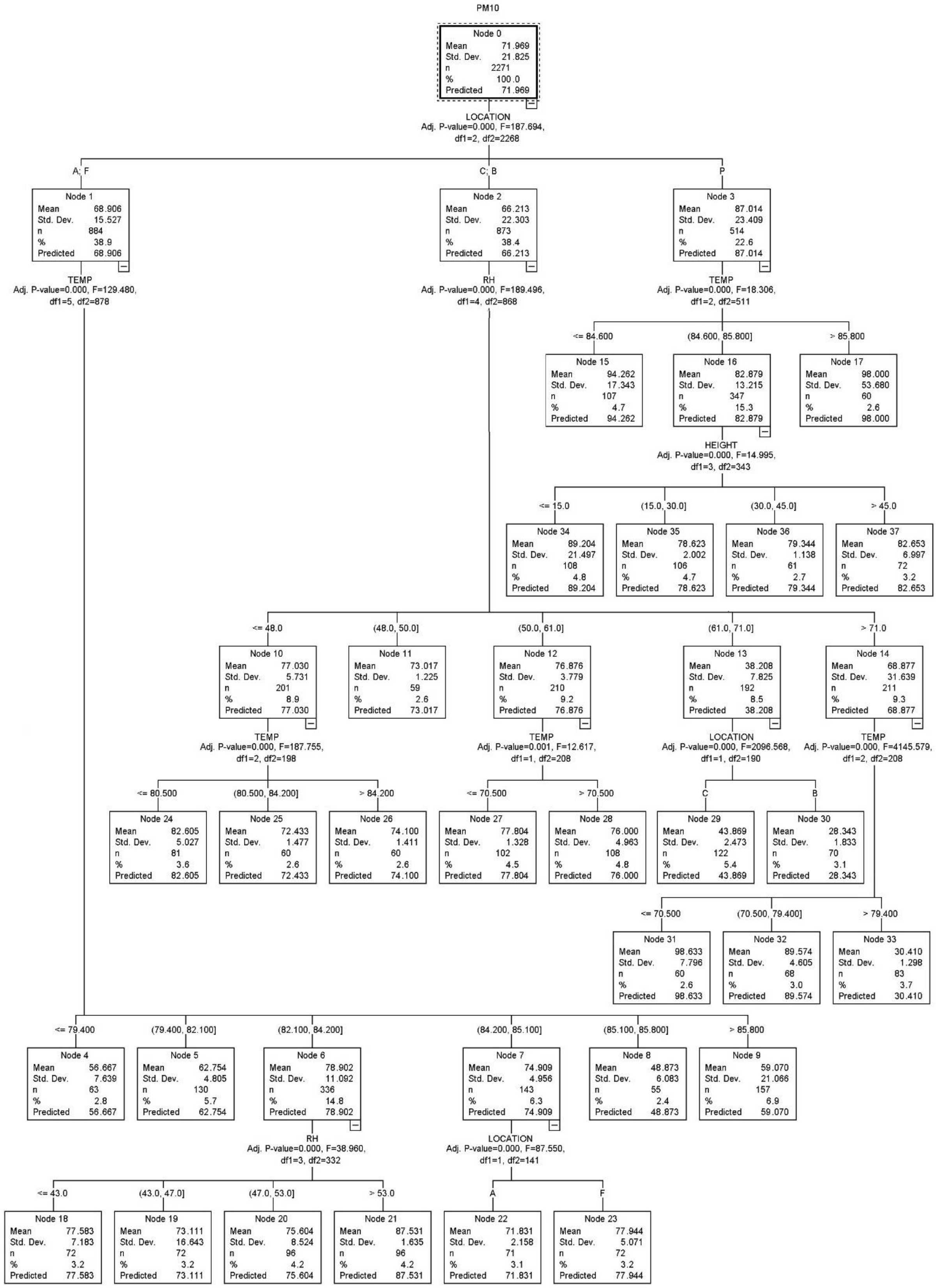

Figure 5. The overall structure of the CHAID DT for PM_{10}

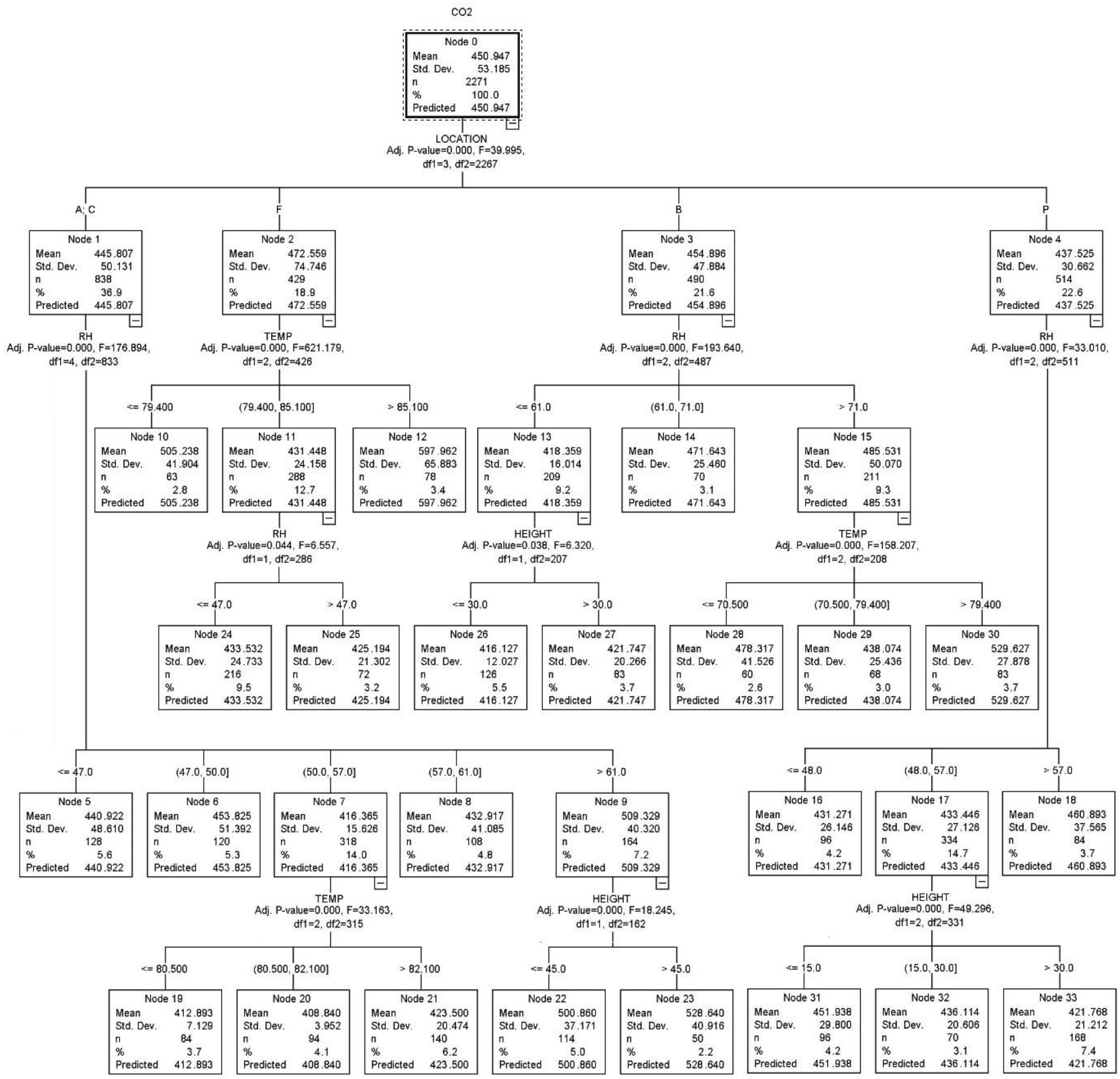

Figure 6. The overall structure of the CHAID DT for CO_2

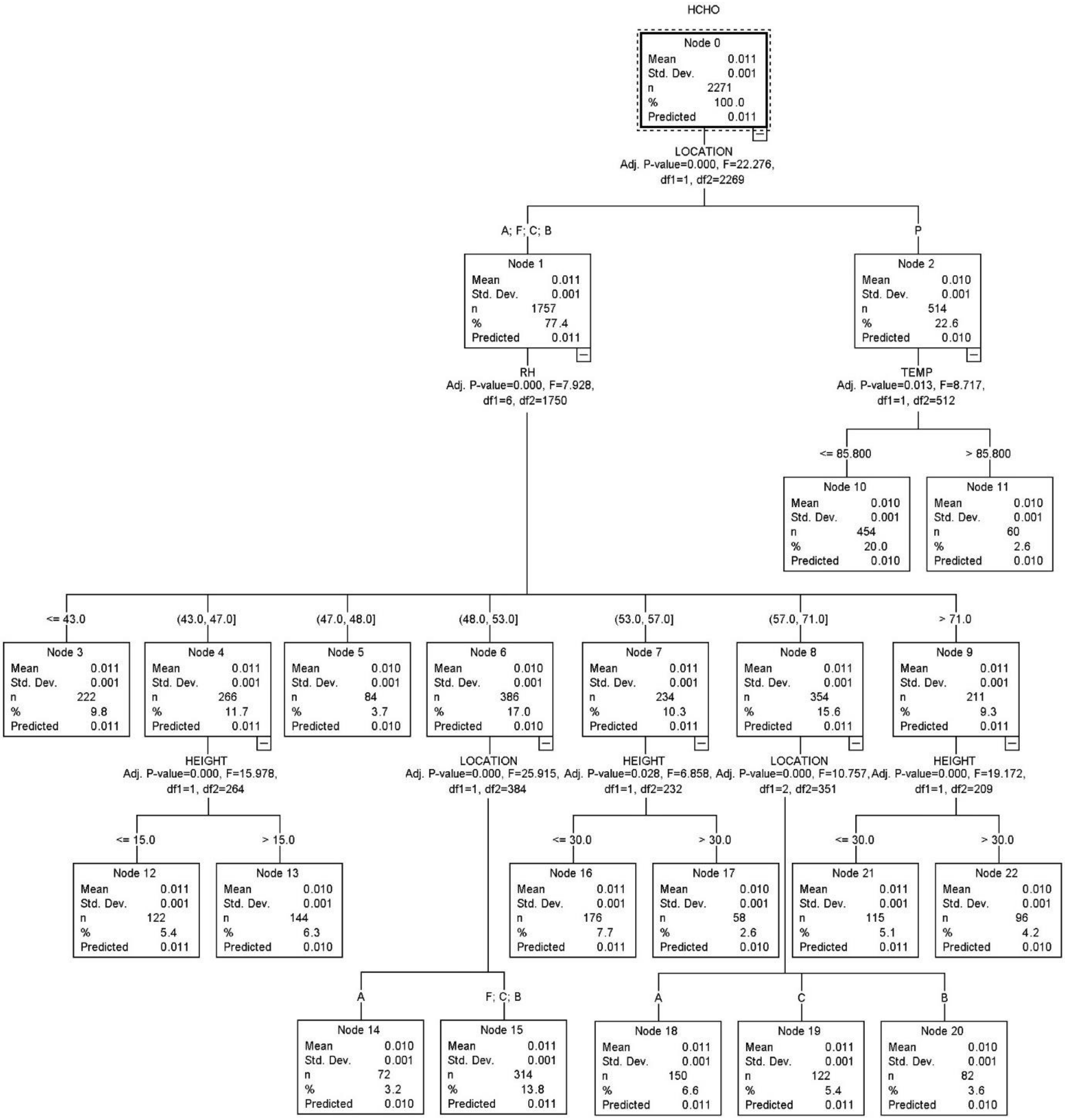

Figure 7. The overall structure of the CHAID DT for HCHO

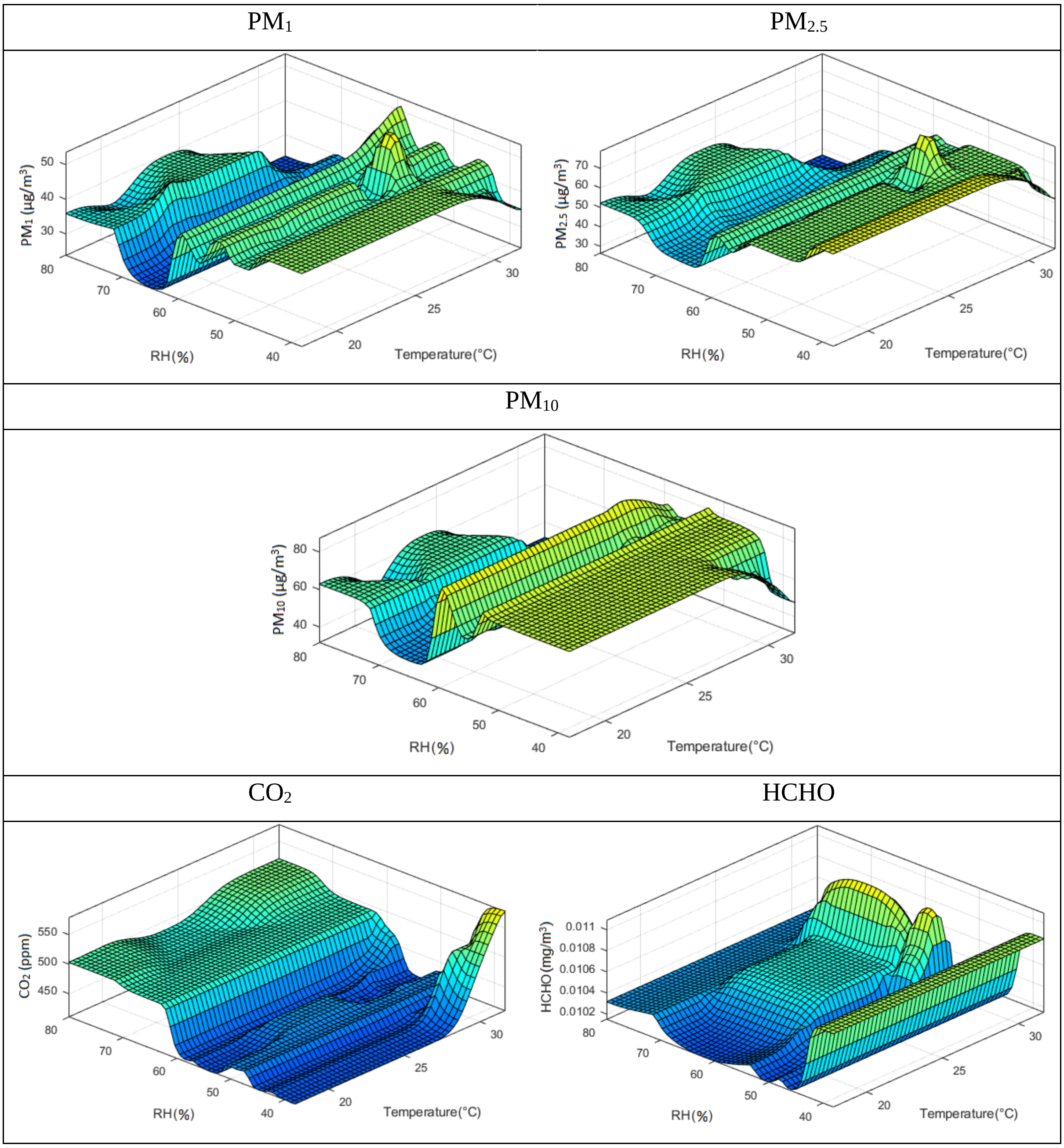

Figure 8. The concentration of pollutants based on *temperature* and *RH*

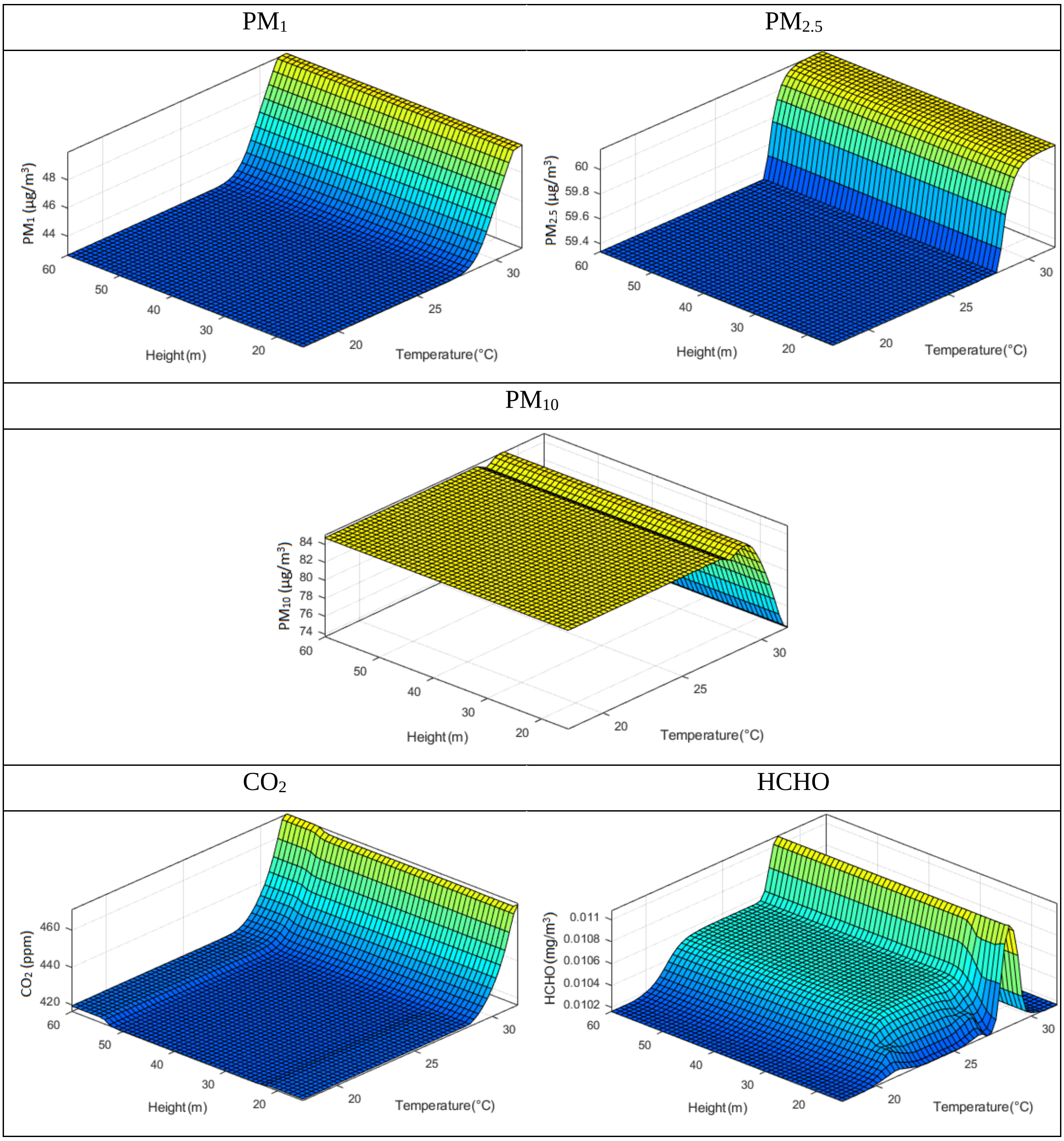

Figure 9. The concentration of pollutants based on temperature and height

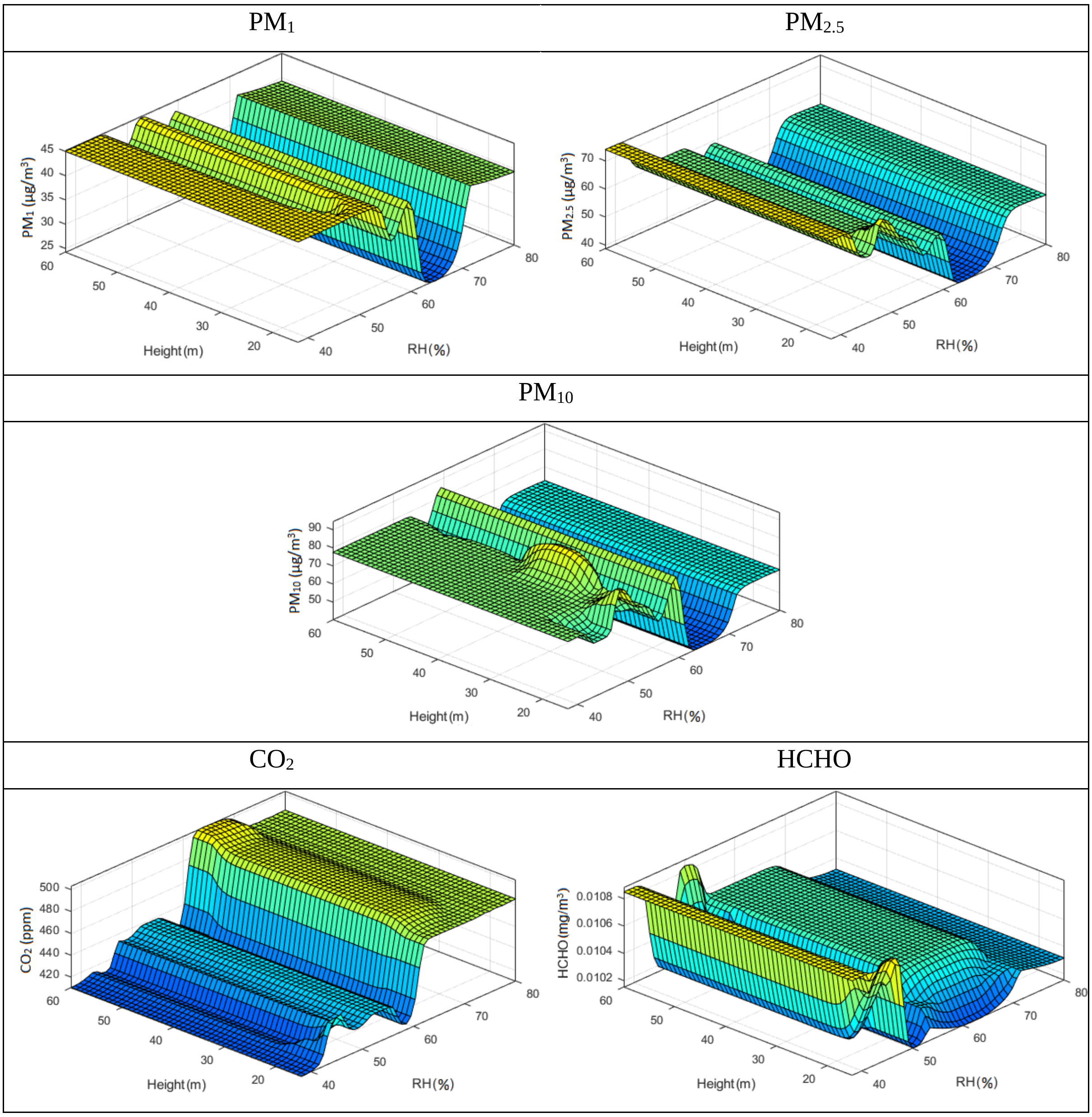

Figure 10. The concentration of pollutants based on *RH* and *height*

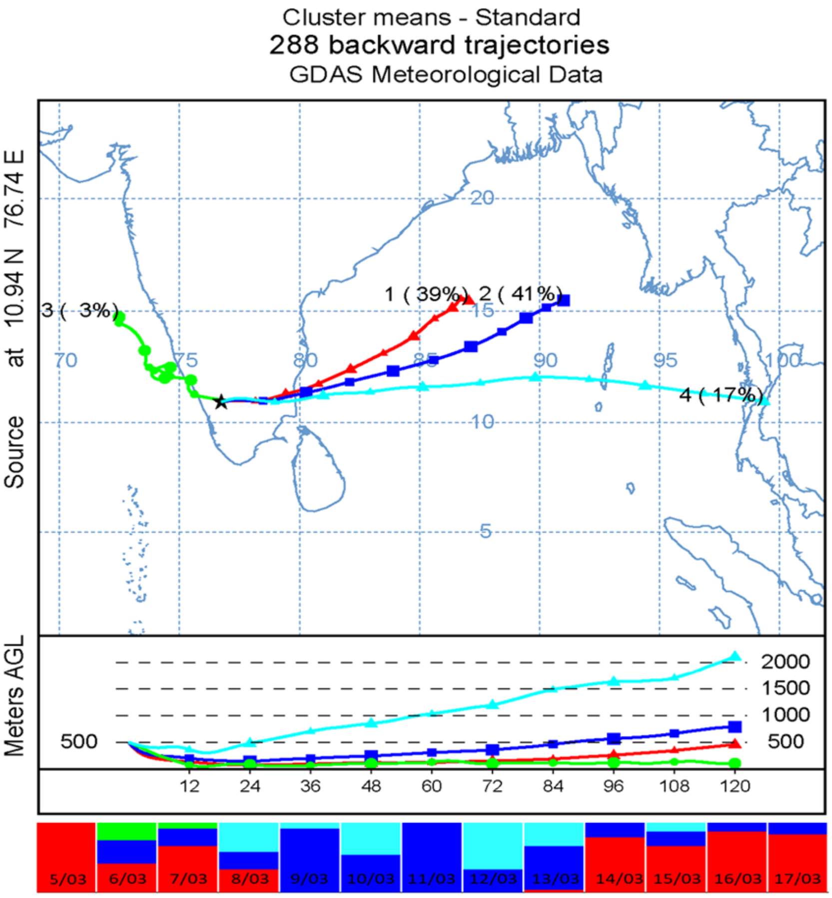

Figure 11. Cluster analysis of five days' hourly air mass back-trajectories arriving at 500 m AGL over the observation site.

Table 1. The sequence of PM_1, $PM_{2.5}$, and PM_{10} concentration in the studied locations in terms of the minimum, lower quartile, mean, upper quartile, and maximum

Value	**Location**	**Pollutant concentration** ($\mu g\ /m^3$)		
		PM_1	**$PM_{2.5}$**	**PM_{10}**
Minimum	Administration Block	25	28	42
	Flight Hangar	18	24	28
	CTC Block	26	34	39
	Bethesda	12	24	26
	Petrol Pump	40	57	73
Lower quartile	Administration Block	36	49	61
	Flight Hangar	34	46	57
	CTC Block	30	38	46
	Bethesda	22	28	31
	Petrol Pump	46	62	78
Median	Administration Block	38	54	67
	Flight Hangar	40	58	73
	CTC Block	42	58	72
	Bethesda	40	58	74
	Petrol Pump	48	63	80
Mean	Administration Block	40.81	55.33	68.68
	Flight Hangar	42.01	55.71	69.14
	CTC Block	40.23	54.11	66.74
	Bethesda	40.21	54.20	65.80
	Petrol Pump	52.79	69.91	87.01
Upper quartile	Administration Block	45	60	74
	Flight Hangar	51.5	66	82
	CTC Block	45	61	76
	Bethesda	49	66	84.25
	Petrol Pump	51.25	67	85

Maximum	Administration Block	58	76	91
	Flight Hangar	63	76	90
	CTC Block	58	73	88
	Bethesda	72	99	123
	Petrol Pump	58	74	94